Heat transfer by oil natural convection in an annular space under combined effects of carbon nanotubes and electric field

Sarra Rejeb, Walid Hassen, Lioua Kolsi, Patrice Estellé

Heat transfer by oil natural convection in an annular space under combined effects of carbon nanotubes and electric field

Sarra Rejeb[a], Walid Hassen[a], Lioua Kolsi[b], Patrice Estellé[c*]

[a] Laboratory of Metrology and Energy Systems, Monastir, University of Monastir, 5000 Monastir, Tunisia
[b] Mechanical Engineering Department, College of Engineering, University of Ha'il, 81451 Ha'il City, Saudi Arabia
[c] Univ Rennes, LGCGM, 35000 Rennes, France

Corresponding author: patrice.estelle@univ-rennes1.fr

ABSTRACT:

In this study, the combined impact of carbon nanotube volume fractions and the electric field on the enhancement of dielectric oil heat transfer is investigated. The geometry studied is an annular layer filled with the dielectric oil and bounded by two eccentric or concentric cylinders. A temperature gradient and an electrical potential difference are applied between the two cylindrical walls. The goal is to analyse the flow behaviour and the heat transfer improvement using a double enhancement technique by combining an active (electric field) and passive (nanoparticles) approach. An in-house numerical simulation code using the finite volume method was developed to solve the set of coupled equations describing the conservation laws of the electro-thermo-hydrodynamic flow associated with the oil. A parametric study, outlining the influence of different relevant variables has been performed. The parameters investigated are the thermal Rayleigh number $(2000 \le T \le 100\,000)$, the electrical Rayleigh number $(100 \le T \le 600)$, the radius ratio $(0.1 \le \Gamma \le 0.9)$, the eccentricity $(0\% \le e \le 90\%)$, the nanotubes volume fraction $(0\% \le \Phi \le 0.5\%)$ and the injection level $(1 \le C \le 10)$ respectively. The effect of these variables on the heat transfer intensification is examined in detail. According to the adopted configuration, heat transfer intensifications between 3% and 77% have been recorded essentially when an electric field was applied. Also, the addition of a 0.5% volume fraction of carbon nanotubes provides a heat transfer improvement of around 27%. Furthermore, for a first time a multiparameter correlation has been developed. This correlation can be useful to better understand the impact of various physical parameters on the heat transfer in annular spaces and also to predict exact values of the Nusselt number.

Nomenclature

a	Thermal diffusivity (m^2/s)
C	Injection strength
Cp	Specific heat at constant pressure (J/kg.K)
E	Electric fields (V/cm)
e	Eccentricity
g	Acceleration of gravity (m/s^2)
j	Electric current density (A/m^2)
K	Ionic mobility ($m^2/V.s$)
M	Mobility number
Nu	Nusselt number
P	Pressure (Pa)

Pr	Prandtl number
q	Electric charge density (C/m^3)
r	Radius (m)
(r,φ)	Cylindrical coordinates
Ra	Thermal Rayleigh number
T	Electric Rayleigh number
t	Time (s)
U	Velocity (m/s)
V	Electric potential (V)

Greek symbols

β	Coefficient of thermal expansion (1/K)
ε	Permittivity of the fluid (F/m)
$\Gamma\left(=r_0/r_i\right)$	Radius ratio
θ	Temperature (K)
λ	Thermal conductivity (W/m.K)
μ	Dynamic viscosity (Pa.s)
ν	Kinematic viscosity (m^2/s)
ρ	Density (kg/m^3)
ϕ	Nanoparticle volume fraction (%)
ψ	Stream function (m^2/s)
ω	Vorticity (1/s)

Subscript

C	Cold
F	Fluid
H	Hot
i	Inner cylinder
nf	Nanofluid
o	Outer cylinder
s	Solid

Superscript

*	Dimensional variables

1. Introduction

Efforts to improve heat exchangers in many industrial sectors (automotive, electronics, power generation, refrigeration, aerospace, etc.) require the intensification of natural convective heat transfer. Phase change materials, metal foam fluid additives, the use of appropriate materials and the modification of the system geometry by the use of differently shaped fins are recent techniques are recent techniques which have generated extensive research attention in the last few years [1]–[3]. Nevertheless, other emerging solutions for heat transfer optimization and intensification, are much less studied, but start to attract the interest of researchers and engineers. Among these techniques, the application of an electric field can be used to create instabilities that initiate motion in a liquid. Here we are dealing with a branch of physics named electro-hydrodynamics (EHD). If the temperature gradient effect is taken into account, the process is called electro-thermo-hydrodynamics (ETHD). In this work, it should be noted that we intend to use an electric field as an active method of

intensification coupled with the addition of nanoparticles in the working fluid as a passive method while hoping to obtain a double enhancement of heat transfer. Indeed, the introduction of nanofluids as thermal fluids is a recognized method to guarantee a good thermal efficiency by modifying the thermophysical characteristics of the fluid.

Electro-thermo-hydro-dynamics (ETHD) is a technique with interesting prospects. Indeed, the first phenomena of heat transfer intensification in liquids and gases were observed by Senftleben and Brawn [4] as early as 1936. They discovered that when an electric field is applied radically between a heated wire and a cylinder, the rate of heat transfer increases by up to 50%. In the early 1950s, Ahmann and Kronig [5] extended the work of Kronig and Schwartz [6] by performing experiments on dielectric liquids and estimated increases in the amounts of heat exchanged. In 2004, Yan et al. [7] performed numerical and mathematical modelling of EHD intensification of free convection in an enclosure, but the problem was partially addressed because the influence of the electrical parameters (electrical force, nature of the fluid, etc.) on the enhancement of the heat transfer was not considered. In 2012, Traoré et al. [8] numerically analysed by the finite volume method, the combined effect of thermal and electric fields on a dielectric fluid layer placed between two parallel planes. It is shown that the electrical effects dominate the buoyancy effects resulting in electrically induced convection, which significantly enhances the heat transfer. Koulova et al. [9] used this same configuration including the temperature dependence of all electrical properties (mobility and electrical permittivity). They also took into account not only the Coulomb force but also the dielectrophoretic force. Both the variation of the Nusselt number and the flow were presented in detail. It is demonstrated that electric charge injection improves heat transfer and that the Nusselt number is unrelated to the thermal Rayleigh number for sufficiently high values electric Rayleigh number. Hassen et al. [10], [11] studied the impact of electrical forces on the behaviour of a dielectric liquid enclosed in an annular space. They asserted that as a result of the implementation of the electric force, the Nusselt number was enhanced up to 170%. In recent years, many researchers have studied electrohydrodynamic thermal instability in dielectric fluids, such as EHD enhanced heat transfer, EHD pump, nanotechnology, etc. Rezaee et al [12] worked on the influence of electro-hydrodynamics forces on natural convection heat transfer; they experimentally examined a rectangular surface equipped with a several vertical fins. They reported that the electrostatic force had a major impact on thermal convection and that an enhancement around 38% in heat transfer was achieved. Fernandes and Suh [13] presented a simple electro-hydrodynamics pump design for dielectric liquids. This pump is perfectly adapted for cooling of electronic equipment. The authors were able to solve the coupled Poisson-Nernst-Planck and Navier-Stokes equations to obtain an analytical solution describing the fluid flow behaviour. Based on the Taguchi method, an optimal design for the EHD pump was developed by considering several geometrical parameters such as length, diameter and position of the electrodes used. Rani et al. [14] worked on the generation of instabilities in a micropolar dielectric liquid layer under the simultaneous action of an alternating electric field and a temperature gradient. They analysed the dependence of

micropolar viscosity and electrical Rayleigh number on convection initiation. It has been proven that the electric field destabilises the convection phenomenon, while conversely the micropolarity helps to stabilise it.

on the other hand, nanofluid technology, has received much attention because of its potential applications in many areas of advanced engineering and nanotechnology, such as microfabrication, nuclear reactor cooling, and microelectronic equipment technology. Furthermore, this technology opens up new possibilities to improve heat transmission efficiency [15]. Maghrabie et al. [16] studied the impact of nanofluids on the performance of heat exchangers. Several types of nanofluids with different natures of nanoparticles (CuO, Fe2O3, Al_2O_3, TiO_2, CNT,...) and several heat exchanger technologies have been presented. In all cases, it has been proved that the addition of nanoparticles improves heat transfer. Radiah et al. [17] studied the contribution of the shape of nanoparticles to the flow of nanofluids. Several types of base fluids (motor oil, ethylene glycol, and water) and nanoparticles (SWCNT, Cu, and Al_2O_3) were tested on a stretched surface in the presence of a thermal and magnetic field. It was noted that the shape change of the nanoparticles has a major effect on the temperature distribution in the studied area and that the sphere shape SWCNTs-ethylene glycol couple presents the highest heat transfer rate compared to all other mixtures. Mallick et al. [18] studied the flow of electrokinetic peristaltic nanofluids using the Eyring-Powell fluid model. They indicate that a higher volume fraction of nanoparticles can significantly improve the momentum transmission in the microchannel core region. Kolsi et al. [19] solved the three-dimensional magnetohydrodynamic free convection in an open cubic cavity filled with a water-CNT nanofluid equipped with a tilted plate. A parametric study based on the variation of the Rayleigh number, the volume fraction of nanoparticles, the Hartmann number, and the angle of inclination of the fins showed that the maximum heat transfer is obtained for a fraction of nanoparticles equal to 0.05%, for a zero Hartmann number, and when the angle of inclination of the fins is equal to 180°. Chand et al. [20] analysed the different thermal instabilities that occur in a horizontal layer of porous medium filled with nanofluid and subjected to a vertical electric field. They applied the Brinkman-Darcy model for the momentum equation and the Brownian diffusion method for the dispersion of nanoparticles. The authors have shown that the Lewis number, the electric field, and the presence of nanoparticles have a destabilizing effect on stationary convection. Hosseinzadeh et al. examined the effect of hybrid nanofluids in a porous medium enclosed in complex cavities. The case of a mixture of water-ethylene glycol as the base fluid with MoS_2-TiO_2 hybrid nanoparticles [21] and the case of 1-Butanol with MoS_2-Fe_3O4 [22] have been extensively investigated. In both cases, Nusselt number improvements of 61.82% and 55.44% respectively were achieved. Kasaeipoor et al. [23] used the Lattice Boltzmann method to study free convection heat transfer and generated entropy analysis of an MWCNT-MgO (15% -85%)/water hybrid nanofluid. In this original work, the thermophysical properties adopted by the authors are derived from experimental

data. They mention that the heat transfer is proportional to the volume fraction of nanoparticles, while the entropy generation is inversely proportional to this content.

The coupling between two heat transfer intensification techniques, namely the use of an electric field as an active method and the inclusion of nanoparticles as a passive method, has rarely been investigated. Among these few works, Asadzadeh et al. [24] examined the free convective heat transfer of Fe_3O_4/Ethylene glycol nanofluids by applying an electric field to a small platinum wire. In this work, the findings revealed that the inclusion of nanoparticles to ethylene glycol improved the heat transfer exchange. The authors also found that highest heat transfer is achieved with a nanoparticle volume fraction of 0.05%. Sheikholeslami et al. [25], [26] dealt with the case of lid-driven enclosure and focused mainly on the study of electric forces in the mixed heat convection of Fe_3O_4 / Ethylene Glycol nanofluids. The authors show that it is possible to reach a significant heat transfer intensification of up to 75%. Hassen et al. [27] considered the case of a square cavity filled with a MWCNT oil-based nanofluid. From numerical analysis, they performed a parametric study by varying the volume fraction of the nanoparticles and the thermal and electrical Rayleigh numbers. It was noted that the use of an electric force and the injection of 0.4% volume fraction of nanoparticles lead to a considerable improvement in heat transfer of around 43%.

The main objective of this work is to numerically study the flow behaviour and the heat transfer enhancement of a CNT-oil nanofluid between two cylinders and under the action of an electric field. This work deals with a double intensification of the heat transfer by combining both an active (electric field) and a passive (nanoparticles) method. Several configurations have been treated, namely the case of low and high injection "C", the effects of radius ratio "Γ", thermal gradient "Ra", eccentricity "e" and applied electrical potential "T". As far as the authors knows, numerical research associated to such coupled effects are extremely rare in the case of EHD flows and non-existent in annular spaces.
The finite volume method of Patankar will be adopted by using an in-house code developed under the Fortran programming language.
It should be noted that in two previous papers [28]-[29] we have numerically studied the annular electro-convection and electro-thermo-convection generated by an electric and/or thermal field. Here, we extend the study to the nanofluid liquid. We will numerically evaluate the heat transfer enhancement by natural convection resulting from the addition of carbon nanotubes in a horizontal annulus.
The remainder of the paper is organized as follows. In Section 2, we present the physical problem, governing equations, and the numerical methods. The Results and discussion are presented in Section 3. Finally, in Section 5, we summarize our findings.

2. Physical model and governing equations

2.1. Configuration and governing equations

The considered geometry is an annular space circumscribed by two infinite and highly conducting cylinders, as illustrated in Fig. 1. A CNT-oil-based nanoliquid is enclosed between the cylinders (Table 1). The CNT is mixed within Newtonian, incompressible and completely insulating thermal oil.

The concentric or eccentric cylindrical walls are assumed to be non-deformable with good thermal conductivity. They are held at set but different temperatures θ_H and θ_C ($\theta_H > \theta_C$). The emitting electrode subjected to high potential V_i corresponds to the hot internal cylinder and represents the electric charge injector electrode. The cold outer cylinder connected to ground is called the collector electrode where the electrical charge will be absorbed ($V=V_0$). In order to avoid undue complexity, the charge injection at the inner cylinder is assumed to be "homogeneous" and "autonomous". This implies that the charge density is identical over the entire cylindrical injector wall and independent of time. In addition, the non-slip boundary conditions (zero velocity on the cylinder walls) are adopted. Since the electric current density is quite low in insulating liquids, Joule heating and viscous dissipation can also be neglected [30]. The Boussinesq approximation, which keeps all physicochemical parameters constant except the density, which is a function of temperature, is also considered.

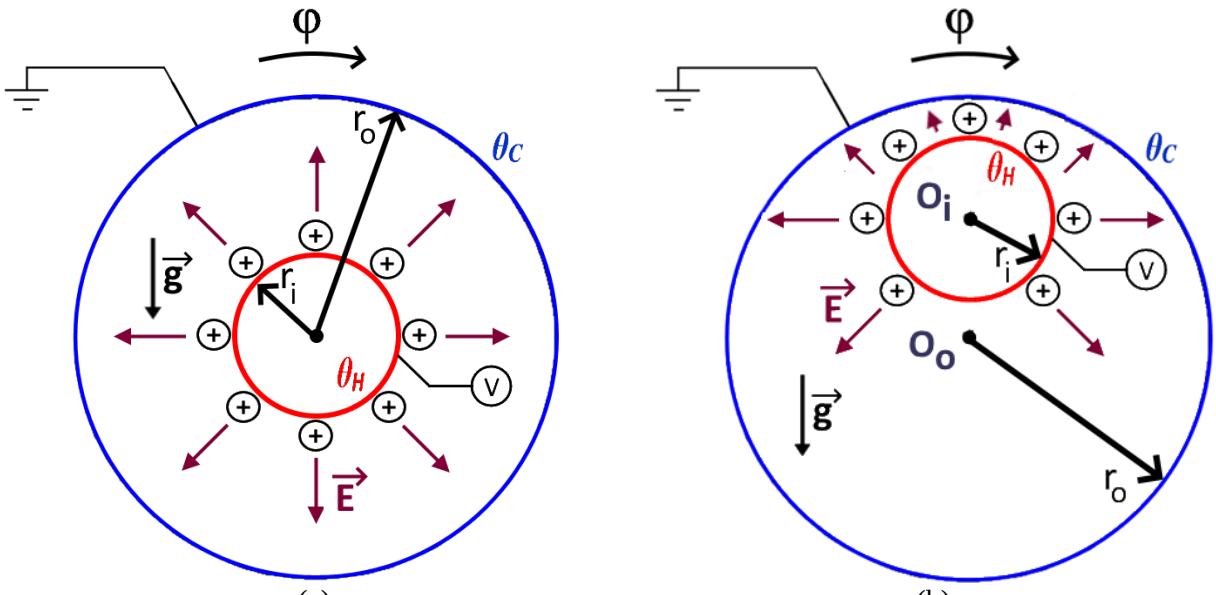

Fig.1. Physical model (a): concentric case, (b): eccentric case

Table 1. Thermophysical characteristics of the base fluid and the nanoparticles [27], [31].

	Thermal oil	**CNT**
Density ρ [kg.m^{-3}] at 15°C	854.5	2100
Specific heat capacity Cp [J.kg^{-1}.K^{-1}] at 45°C	1970	733

Thermal conductivity k [$W.m^{-1}.K^{-1}$] at 35°C	0.133	2000
Coefficient of thermal expansion β [$°C^{-1}$]	$7.688\ 10^{-4}$	10^{-7}
Viscosity ν [m^2/s] at 40 °C	$4\ 10^{-6}$	--

The governing equations used in this work are as follows [27] [32]:

The mass conservation equation

$$\nabla \cdot \vec{U} = 0 \tag{1}$$

The Navier-Stokes equations

$$\rho_{nf}\left(\frac{d\vec{U}}{dt} + \vec{U}\cdot\nabla\vec{U}\right) = -\vec{\nabla}p + \mu_{nf}\nabla^2\vec{U} + \rho_{nf}\vec{g}\beta_{nf}\left(\theta-\theta_0\right) + q\vec{E} \tag{2}$$

The energy equation

$$(\rho C_p)_{nf}\left(\frac{d\theta}{dt} + \vec{U}\cdot\nabla\theta\right) = k_{nf}\nabla^2\theta \tag{3}$$

The charge conservation equation

$$\frac{\partial q}{\partial t} + \nabla.\left(qK\vec{E} + q\vec{U}\right) = 0 \tag{4}$$

The Gauss's law equation

$$\nabla\cdot\left(\varepsilon\vec{E}\right) = q \tag{5}$$

The definition equation for electric field

$$\vec{E} = -\nabla V \tag{6}$$

The eccentricity "e" is defined by

$$\mathrm{e} = \frac{\overline{\mathrm{O_iO_o}}}{\left(\mathrm{r_o}-\mathrm{r_i}\right)} \tag{7}$$

The centres of the inner and outer cylinders are represented by Oi and Oo, respectively.

The effective thermophysical properties of CNT- thermal oil [31], [33]:

- The density

$$\rho_{nf} = \rho_f(1-\Phi) + \rho_s\Phi \tag{8}$$

- The viscosity

$$\mu_{nf} = -1.8231 - \frac{0.0686}{\theta} + 1.7235\left(1-\Phi\right) + 3.329\left(1-\Phi\right)^2 + 136.7838\frac{\left(1-\Phi\right)^2}{\theta^2} - 3.2363\left(1-\Phi\right)^3 - 2347.39\frac{\left(1-\Phi\right)}{\theta^3} \tag{9}$$

- The thermal conductivity

$$k_{nf} = 0.595 - 0.4547\left(1-\Phi\right) + \theta\left(0.7422 - 0.606\left(1-\Phi\right) + \frac{0.2759}{\left(1-\Phi\right)} - \frac{0.3943}{\left(1-\Phi\right)^2} \right) \tag{10}$$

- The specific heat [kJ.kg^{-1}.K^{-1}]

$$Cp_{nf} = -20 + 21.573\left(1-\Phi\right) - 0.012\ \theta + 0.024\ \theta\left(1-\Phi\right) \tag{11}$$

- The thermal expansion coefficient

$$\beta_{nf} = 7.56\ 10^{-4} + 6.34\ 10^{-7}\theta - 8.09\ 10^{-4}\left(1-\Phi\right) \tag{12}$$

For universal modelling, the following dimensionless parameters are defined:

$$E^* = E\frac{r_o - r_i}{V_i - V_o} \qquad r^* = \frac{r}{r_o - r_i} \qquad U^* = U\frac{r_o - r_i}{a} \qquad \psi^* = \frac{\psi}{a} \qquad \omega^* = \omega\frac{\left(r_o - r_i\right)^2}{a} \qquad t^* = t\frac{a}{\left(r_o - r_i\right)^2}$$

$$\theta^* = \frac{\theta - \theta_C}{\theta_H - \theta_C} \qquad q^* = \frac{q}{q_i} \qquad V^* = \frac{V - V_O}{V_i - V_o}$$

Adopting the "stream function-vorticity" formalism (ψ-ω) in cylindrical coordinates (r, φ), the equation system (1) - (6) becomes:

$$\omega = -\left(\frac{\partial^2\psi}{\partial r^2} + \frac{1}{r}\frac{\partial\psi}{\partial r} + \frac{1}{r^2}\frac{\partial^2\psi}{\partial\varphi^2} \right) \tag{13}$$

$$\begin{aligned} \frac{\partial\omega}{\partial t} + U_r\frac{\partial\omega}{\partial r} + \frac{U_\varphi}{r}\frac{\partial\omega}{\partial\varphi} = \frac{\mu_{nf}/\mu_f}{\rho_{nf}/\rho_f}\mathrm{Pr}.\nabla^2\omega + \frac{\beta_{nf}}{\beta_f}Ra.\mathrm{Pr}\left(\sin\varphi\frac{\partial\theta}{\partial r} + \frac{1}{r}\cos\varphi\frac{\partial\theta}{\partial\varphi} \right) \\ + \frac{\rho_{nf}}{\rho_f}\frac{CT^2}{M^2}.\mathrm{Pr}\left(\frac{1}{r}\frac{\partial\left(rqE_\varphi\right)}{\partial r} - \frac{1}{r}\frac{\partial\left(qE_r\right)}{\partial\varphi} \right) \end{aligned} \tag{14}$$

$$\frac{\partial\theta}{\partial t} + U_r\frac{\partial\theta}{\partial r} + \frac{U_\varphi}{r}\frac{\partial\theta}{\partial\varphi} = \nabla^2\theta \tag{15}$$

$$\frac{\partial q}{\partial t} + \frac{1}{r}\frac{\partial}{\partial r}\left(qr\left(U_r + Ra.\mathrm{Pr}.E_r\right)\right) + \frac{1}{r}\frac{\partial}{\partial\varphi}\left(q\left(U_\varphi + Ra.\mathrm{Pr}.E_\varphi\right)\right) = 0 \tag{16}$$

$$\frac{\partial^2 V}{\partial r^2} + \frac{1}{r}\frac{\partial V}{\partial r} + \frac{1}{r^2}\frac{\partial^2 V}{\partial\varphi^2} = -C.q \tag{17}$$

$$E_r = -\frac{\partial V}{\partial r} \tag{18}$$

$$E_\varphi = -\frac{1}{r}\frac{\partial V}{\partial\varphi} \tag{19}$$

The radial and orthoradial velocity components can be calculated by:

$$U_r = \frac{1}{r}\frac{\partial \psi}{\partial \varphi} \tag{20}$$

$$U_\varphi = -\frac{\partial \psi}{\partial r} \tag{21}$$

For better readability, the superscript "*" has been eliminated from the dimensionless equations (13)-(21).

Five dimensionless numbers arise in the above equations, they are defined as follows:

The electric Rayleigh number $T = \dfrac{\varepsilon\ \Delta \mathrm{V}}{\rho_f \nu_f K} = \dfrac{\text{destabilizing electrical force}}{\text{stabilizing viscous force}}$

The thermal Rayleigh number $Ra = \dfrac{\mathrm{g}\ \beta_f\ \Delta\theta(\mathrm{r_0}\text{-}\mathrm{r_i})^3}{\nu_f a_f} = \dfrac{\text{destabilizing thermal buoyancy force}}{\text{stabilizing viscous force}}$

The Prandtl number $\mathrm{Pr} = \dfrac{\nu_f}{a_f} = \dfrac{\text{momentum diffusivity}}{\text{thermal diffusivity}}$

The injection strength $C = \dfrac{q_i \left(r_o - r_i\right)^2}{\varepsilon\ \Delta \mathrm{V}}$

The mobility parameter $M = \dfrac{1}{K}\sqrt{\dfrac{\varepsilon}{\rho_f}} = \dfrac{\text{hydrodynamic mobility}}{\text{ionic mobility}}$

2.2. Boundary conditions

The related non-dimensional boundary conditions for fluid stream function, vorticity, temperature, electric potential and charge density at the inner and the outer cylinders are:

For $\mathrm{r} = \mathrm{r_i}$ and $0 \le \varphi \le 2\pi$

$$\Psi = \frac{\partial \Psi}{\partial \mathrm{r}} = 0 \qquad \theta = 1 \qquad \mathrm{V} = 1 \qquad \mathrm{q} = 1 \qquad \omega = \frac{\partial^2 \Psi}{\partial \mathrm{r}^2} = 0$$

For $\mathrm{r} = \mathrm{r_0}$ and $0 \le \varphi \le 2\pi$

$$\Psi = \frac{\partial \Psi}{\partial r} = 0 \qquad \theta = 0 \qquad \mathrm{V} = 0 \qquad \frac{\partial \mathrm{q}}{\partial \mathrm{r}} = 0 \qquad \omega = \frac{\partial^2 \Psi}{\partial r^2} = 0$$

The local and average Nusselt numbers are defined respectively as:

$$\mathrm{Nu_{loc}} = -\left(\frac{\mathrm{k_{nf}}}{\mathrm{k_f}}\right)\mathrm{r_i}\ln\left(\frac{\mathrm{r_o}}{\mathrm{r_i}}\right)\left.\frac{\partial \theta}{\partial \mathrm{r}}\right|_{\mathrm{r=r_i}} \tag{22}$$

$$Nu_{av} = \frac{1}{2\pi}\int_0^{2\pi} Nu_{loc} d\varphi \tag{23}$$

2.3. Code validation and numerical procedure

The entire domain is divided into thousands of tiny control volumes on which all equations (12)-(18) have been discretised by applying the finite volume method (FVM). A semi-implicit first order Euler time scheme is retained to discretize the temporal derivatives [34]. The obtained nonlinear algebraic equations are solved with the iterative successive over relaxation (SOR) algorithm [35]. Indeed at high electric Rayleigh number to avoid the divergence of the computation, Ψ, ω, θ, V and q are under-relaxed. At low electric Rayleigh number in order to accelerate the calculation, Ψ is over-relaxed, whereas ω, θ, V and q are under-relaxed.

The power-law scheme for treating convective terms was adopted with a uniform mesh size of 121x121 nodes. The numerical approach is further discretised in time with a step size of 10^{-4} which ensured the stability of the computations [36].

The FORTRAN platform was chosen in order to build a numerical house code.

The main structure of our solver, for one iteration loop k, is as follows:

Step 0 The initial conditions for all dependent variables are set to zero

Step 1 Solve vorticity Eq. (14)

Step 2 Solve the stream function Eq. (13).

Step 3 Estimate the velocity profile Eq. (20) and Eq. (21).

Step 4 Solve the transport equation for the charge density Eq. (16), and the energy Eq. (15) takes into account the new velocity profile (estimated in the previous step).

Step 5 Solve the electric potential Eq. (17) and extract the components of the electric field Eq. (18) and Eq. (19).

Steps 1–5 are re-executed until the stopping criterion of the SOR loop Eq. (24) is satisfied

$$\frac{\max\left|\psi^{k}-\psi^{k-1}\right|}{\max\left|\psi^{k}\right|}+\frac{\max\left|\theta^{k}-\theta^{k-1}\right|}{\max\left|\theta^{k}\right|}+\frac{\max\left|q^{k}-q^{k-1}\right|}{\max\left|q^{k}\right|}\leq 10^{-5} \tag{24}$$

The interested reader might refer to [10] and [37] for further information on the numerical approach.

To minimize the dependency between the results and the adopted mesh size, a sensitive mesh size analysis is performed for $Ra = 10^4$, $T = 300$, thermal oil fluid ($M = 49$, $Pr = 116.59$), strong charge injection ($C = 10$), $\Gamma = 0.2$ and $\phi = 0.5$. As presented in Table 2, five grids have been

considered. The gap between the 101x201 and 151x301 meshes is 0.31% while the difference between 151x301 and 201x401 meshes is only 0.18%. Therefore, a grid structure with 101x201 cells appears to be a good balance between calculation time and result accuracy.

Table 2. Mesh sensitivity test

Mesh	Nu_{av}	Percentage increase	Incremental increase
51x101	7.8083	-	-
81x161	8.0168	2.67%	-
101x201	8.1138	3.91%	1.21%
151x301	8.1389	4.23%	0.31%
201x401	8.1535	4.42%	0,18%

For further validation, a quantitative comparison can be seen in Figure 2, in which the experimental (Kuehn and Goldstein [38]) and numerical (present work) radial temperature distribution is plotted. As demonstrated in this figure, our numerical results are in quite good accordance with the experimental data with a deviation not exceeding 1.5%.

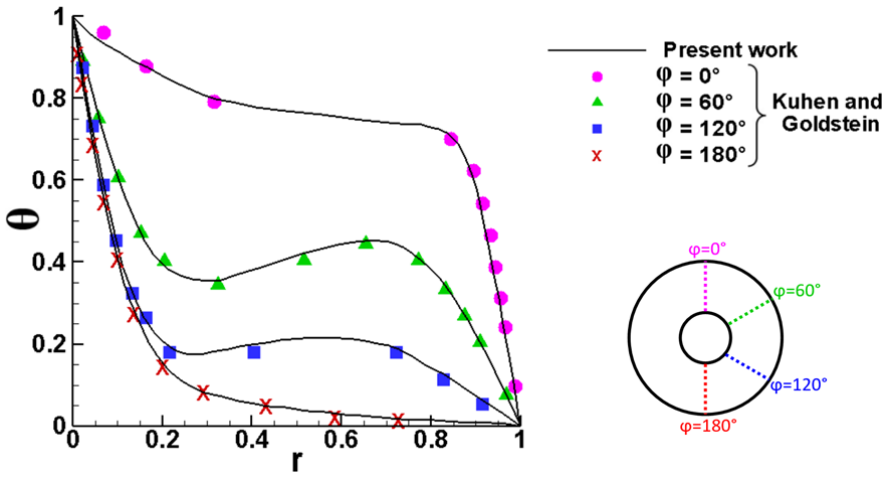

Fig. 2 Comparison of the radial temperature for different angle position with those presented in Ref.[38] (*Pr=0.7, Ra=4.7 10*^{4} *and* Γ=0.3846).

To validate the code from the electro-convection point of view (Figure 3), we have compared our results with those of the analytical ones. Indeed, for a homogeneous and autonomous charge injection between two concentric cylinder electrodes in the hydrostatic regime, an

analytical solution exists. This solution is expressed for the charge density and for the radial electric field as follows [39]:

For $r \in [r_i, r_o]$ with $r_i = \frac{\Gamma}{1-\Gamma}$ and $r_o = \frac{1}{1-\Gamma}$

$$q_s(r) = \frac{A}{C\sqrt{r^2 + B}} \tag{25}$$

$$E_s(r) = \frac{A}{r}\sqrt{r^2 + B} \tag{26}$$

The coefficients *A* and *B* of equations (25) and (26) are reported in Table 3.

Table 3. Coefficient *A* and *B* for the hydrostatic analytic solution of eq. (25) and (26) [39]

Γ	0.1	**0.2**	0.3	0.4	0.5	0.6	0.7	0.8	0.9
A	1.009	**1.099**	1.193	1.302	1.439	1.622	1.886	2.325	3.309
B	-0.0022	**-0.050**	-0.169	-0.427	-0.979	-2.224	-5.409	-15.946	-80.890

Complete agreement between the analytical and numerical solution for the radial distribution of the electric field and the electric charge density is found.

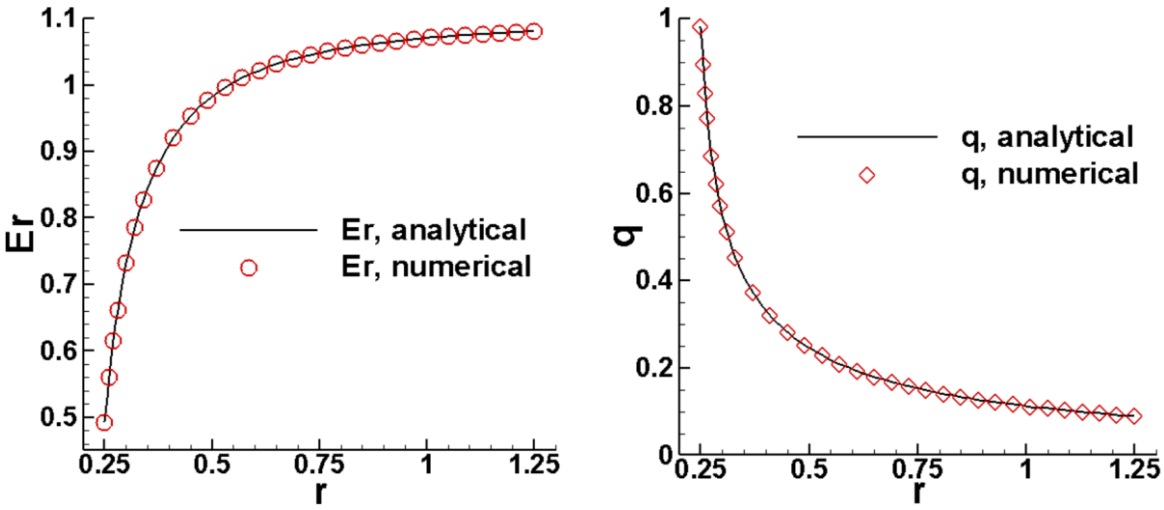

Fig. 3 Comparison between analytical and numerical solution of hydrostatic state for Γ=0.2, e=0, T= 30, C = 10: (a) electric field, (b) charge density.

3. Results and discussion

In this work, a computational analysis has been conducted to study the electrothermal convection phenomenon driven by a strong unipolar injection between two eccentric or concentric cylinders filled with nanofluid composed of insulating oil and CNTs. Several

parameters including electric Rayleigh number, thermal Rayleigh number, eccentricity, electric injection level, nanofluid volume fraction, and radius ratio were analysed.

Fig. 4 presents the electric charge density, the flow structure and the temperature field for ϕ=0.5%, Γ=0.2 and Ra=5000.

As can be seen in this Figure for T = 100, the isothermal lines show the development of a single thermal plume distribution at the top of the annulus. In the whole lower part, the heat transfer is purely conductive giving rise to the so-called dead zone (area of poor heat exchange). In this case, the fluid viscosity counterbalances the electrical force, and the flow is purely generated by the thermal buoyancy forces. A flow similar to the classical natural convection is then obtained. Indeed, two counter-rotating cells with a vortex centre positioned at the bottom of the annular space take place. In fact, the dominant ascending thermal drive the electric charges upwards in the annulus and leads to the emergence of an electric mushroom.

By increasing the T (=250) parameter, the electric force and the buoyancy force are then of the same order, a secondary motion with an electrical drift speed KE takes place. This additional velocity allows the production of another mushroom-shaped plume located in the basal zone of the annulus. Two other small counter-rotating cells are established at the bottom of the annular space and thus help to eliminate the dead zone. A transition from a conductive to a convective regime can then be identified under the inner cylinder.

When T reaches 300 the regime becomes electrically dominated. Indeed, the electrical forces (Coulomb force) are so strong that the drift velocity KE overcomes both the viscous and thermal forces. Three identical and equidistant electric mushrooms appear and establish a multicellular flow. This flow is composed of several symmetrical counter-rotating cells. The charge distribution profile is easy to understand as the Coulomb force is the main driving force because of high T value. The stream function field and charge void region is close to the one we obtained in pure EHD problem, and the temperature can be seen as a passive transport variable. It can be concluded that the number and shape of plumes as well as the flow behaviour (cell size, intensity, and number) are strongly impacted by the electrical Rayleigh value.

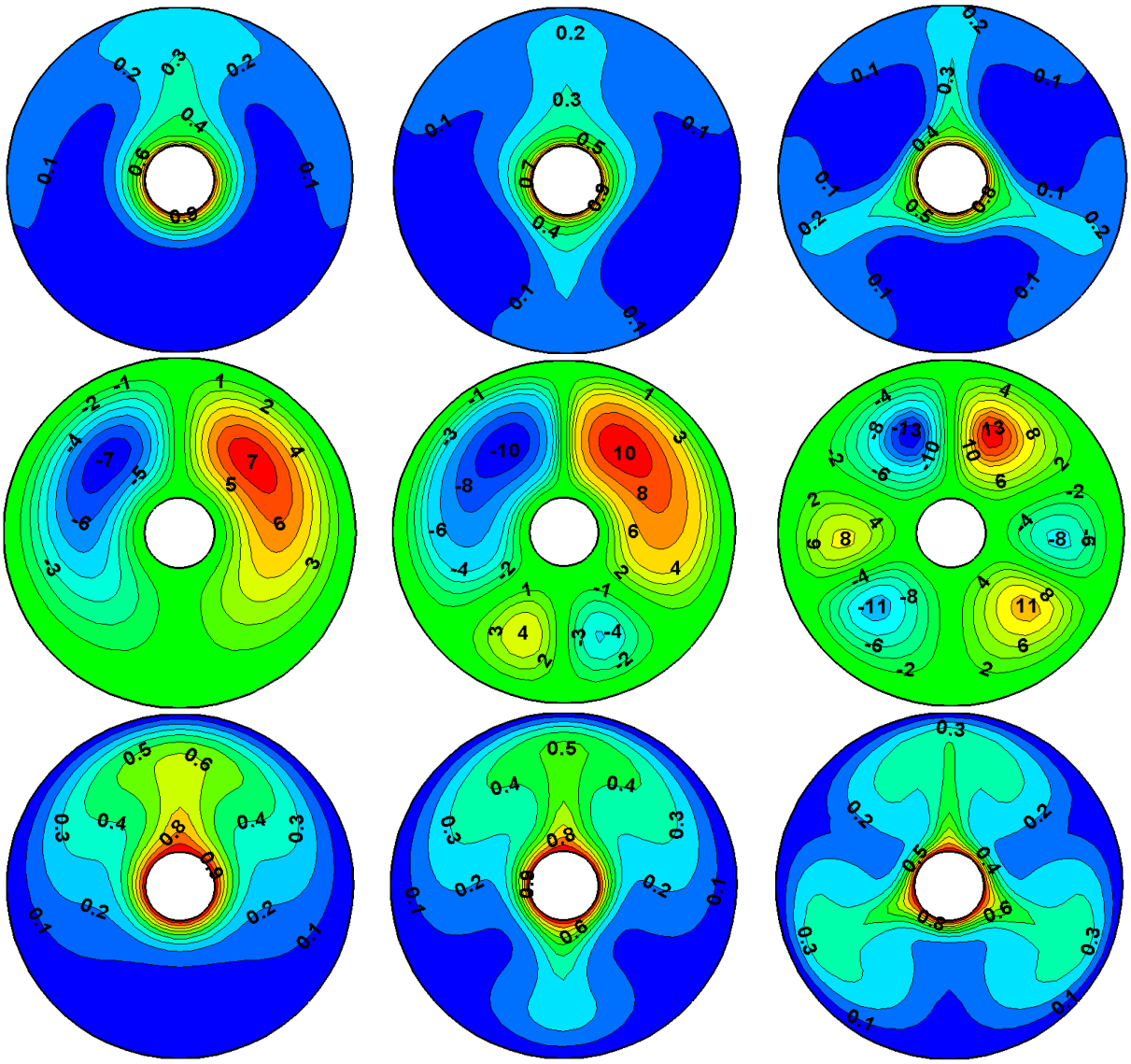

Fig.4. Charge density distribution (top), stream function (middle) and isothermal lines (bottom) for ϕ=0.5%, Γ=0.2, C=10, e=0%, Ra=5000 and different T.

Figure 5. shows the evolution of the electric charge density, the flow structure and the temperature field *Ra*=5000, *C*=10, ϕ=0.5%, *T*=300, *e*=0% and different radius ratio Γ.

As confirmed in the previous figure, for large values of T, the ionic migration causes the circulation of electric charge nets along preferential paths. Electro-convective currents having a mushroom shape are thus generated. The number, size and intensity of these mushrooms are strongly related to the width of the annular layer. It should be noted that increasing the internal cylinder radius enables on one hand to increase the exchange surface and on the other hand to approach the emitter electrode towards the receiver one. These two factors give rise to a greater charge injection with an electric mushroom shape. Indeed, as seen in Fig. 5 the

parameter Γ is proportional to the number of electro-convective mushrooms but inversely proportional to their sizes and intensities. It is also noticed that the charge density gradient is quite high along the angular direction. Indeed, a significant variation of q is recorded by comparing the region between the plumes where the dielectric fluid layer is completely free of electric charge and the centre of a mushroom.

It is also necessary to highlight that since the regime is electrically dominated (high T value), the isotherm lines are almost a carbon copy of the charge density distribution with the same number, same position, and same size of thermal and electrical mushrooms. On the flow side, it is important to mention that each plume will create on both sides two opposite cells. This leads to a multicellular regime composed by several counter rotating cells. It is noted that such symmetrical cells are characterised by a hexagonal shape. The number of these cells goes from 6 to 12 to 26 when Γ goes from 0.2 to 0.5 to 0.8 respectively.

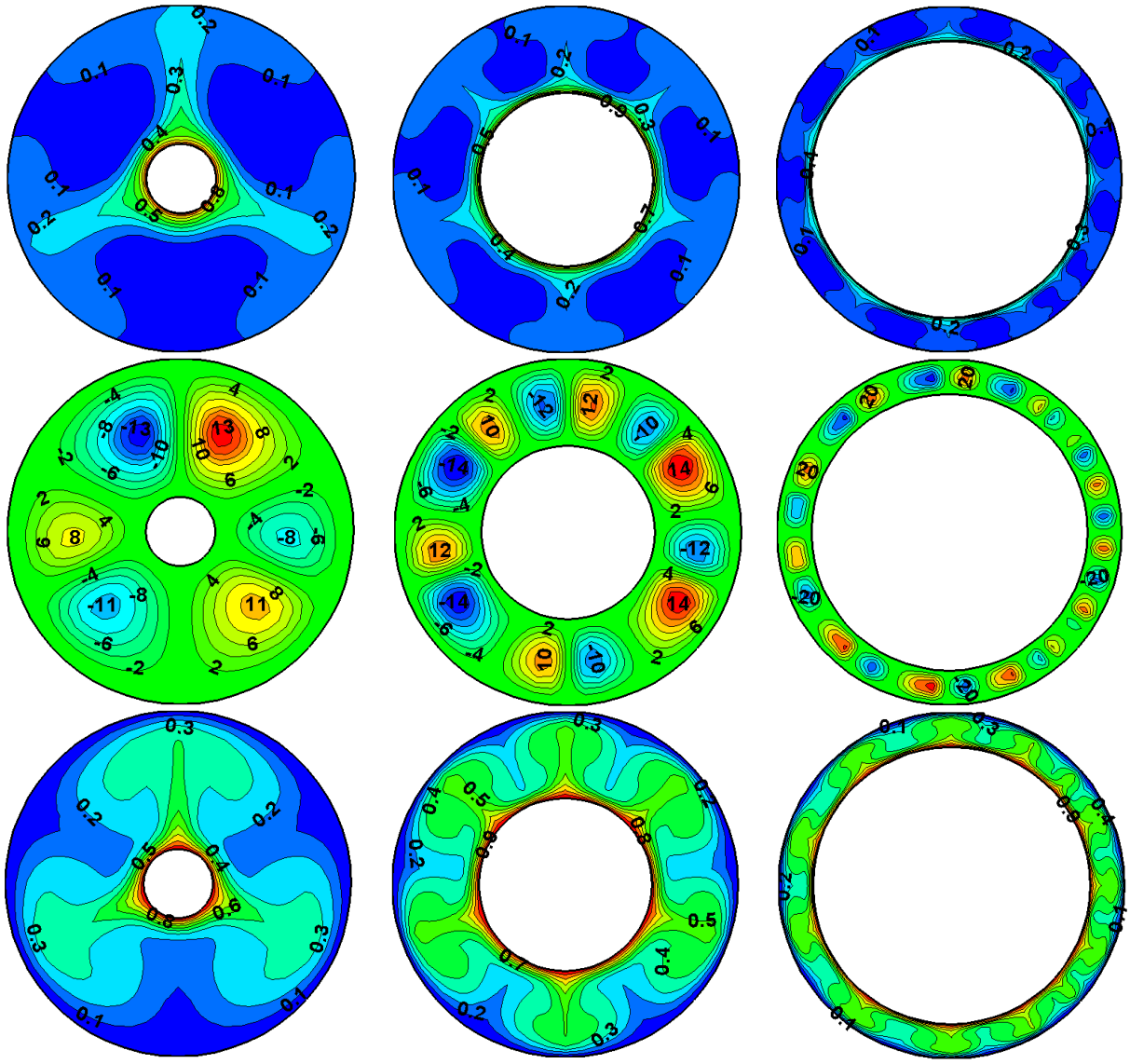

Γ= 0.2 Γ = 0.5 Γ = 0.8

Fig.5. Charge density distribution (top), stream function (middle) and isothermal lines (bottom) for Ra=5000, C=10, ϕ=0.5%, T=300, e=0% and different Γ.

The effect of the injection strength on the charge density distribution is illustrated in Fig.6. Three injection levels were tested, *C*=7 for a strong injection, *C*=3 for a medium injection and *C*=1 for a weak injection respectively. It is clear that the lower the injection level, the more electrical charges penetrate the vacant spaces. Indeed, at *C*=0.1 all the annular space is completely submerged by electrical charges. This could be explained by the fact that for a low injection level the Columbian repulsion between the charge carriers becomes negligible. Therefore, charge inertial forces are exhausted (KE→0) and diffusion becomes the dominant propagation mode. Under these conditions, the charges have enough time to propagate and overwhelm all the cavity.

Moreover, as the injection level decreases, the electrical forces become weaker compared to the thermal ones. Hence, a transition was observed from a multicellular regime (6 cells) for *C*=7 to an intermediate regime (4 cells) for *C*=3 to a bicellular regime for *C*= 0.1. Finally, it is pointed out that with a low *C* value, there is a reappearance of the dead zone of low heat exchange located just under the internal cylinder.

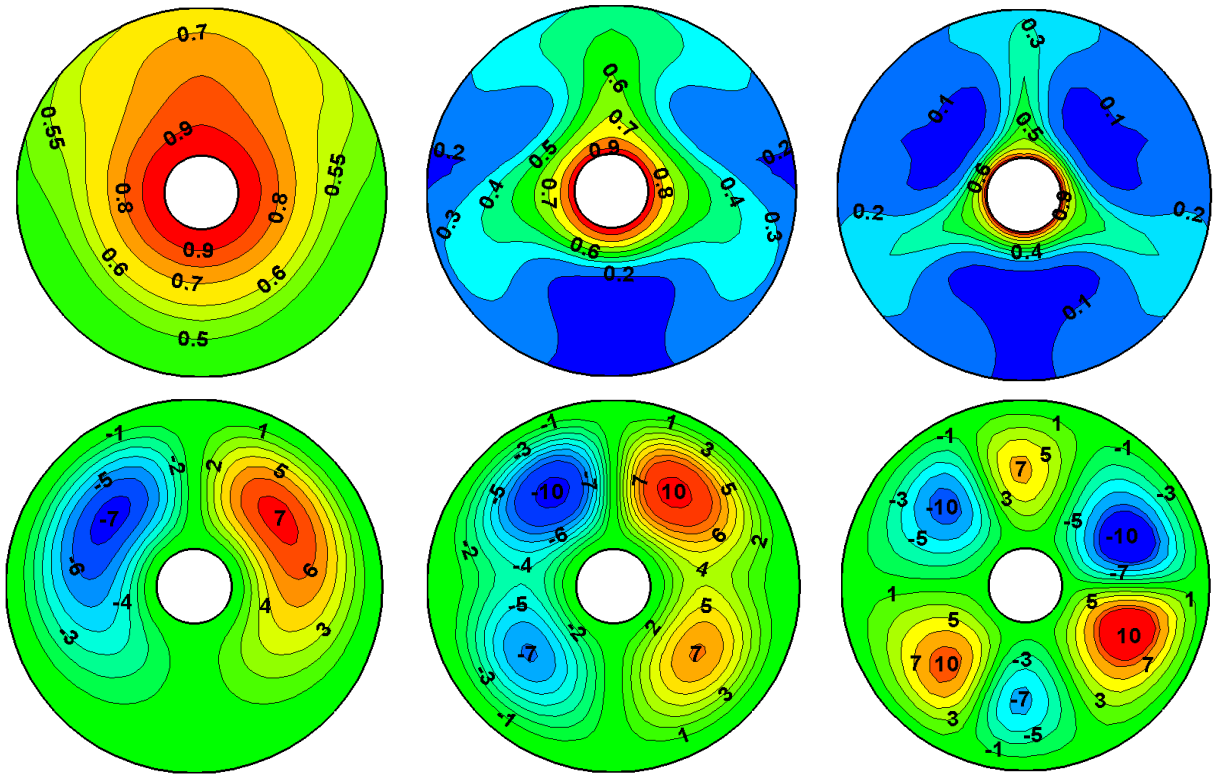

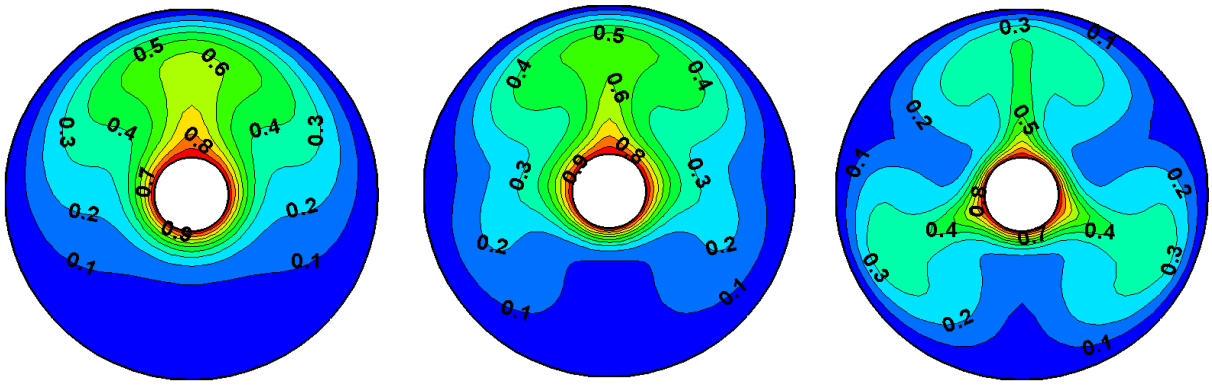

C=1 C=3 C=7

Fig.6. Charge density distribution (top), stream function (middle) and isothermal lines (bottom) for Ra=5000, e=0%, ϕ=0.5%, Γ=0.2, T=300 and different C.

In Figure 7, the charge density distribution according to the eccentricity demonstrates that for downward eccentricity, an intense and dominant electric mushroom located in the basal zone of the annular space takes place; this mushroom is caused by the intense electrical forces produced mainly by the approach of the emitting electrode (inner cylinder) to the receiving electrode (outer cylinder). Another less important plume in the top zone is supplied thanks to the thermal forces. In fact, these buoyancy forces are strong enough to generate convective motion and thereby drive electrical charges into the upper part of the annulus. All this generates a particular flow composed of two large high-velocity cells located above the inner cylinder and two other small, low-velocity cells at the bottom of the cavity, on both sides of the inner cylinder. For upward eccentricity the thermal and electrical forces are concentrated mainly at the top of the annulus. It should be noted that almost all electrical charges are concentrated in the somital area, and weak penetration can be found at the lower part of the internal cylinder. Here also, four counter-rotating cells with the same intensity but different sizes take place in the annular cavity. Concerning the isothermal lines, the hot layers remain localized at the top of the annulus where a very strong thermal gradient is recorded. A very slight intrusion of warm fluid is also detected under the inner cylinder.

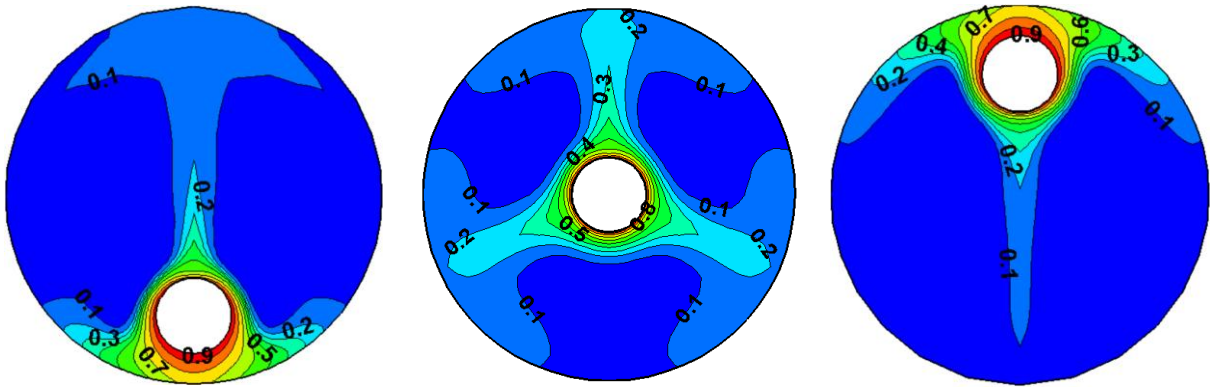

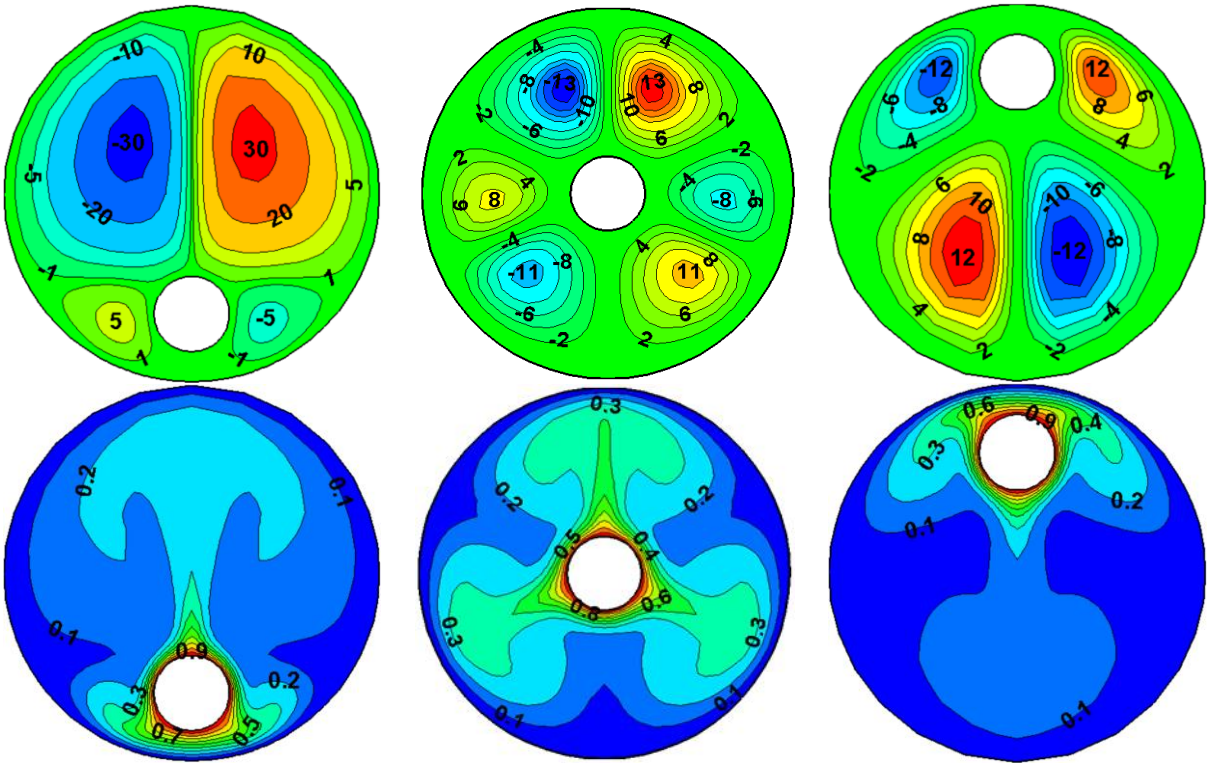

Fig.7. Charge density distribution (top), stream function (middle) and isothermal lines (bottom) for Ra=5000, C=10, ϕ=0.5%, Γ=0.2, T=300 and different eccentricity e.

The temporal progression of the mean Nusselt number for different thermal Rayleigh number values is plotted in Figure 8. The convection heat exchange is clearly proportional to the Ra, as expected. Indeed, changing the Rayleigh number from 5000 to 100000 results in a 40% improvement. The impact of the electrical Rayleigh number on heat transfer is more significant compared to the thermal Rayleigh number. Indeed, as shown in Figure 9, a variation of T from 0 to 600 leads to a Nusselt intensification of about 77%. The addition of carbon nanotube (CNT) (figure 10) allows to enhance the Nusselt number. 27% of heat transfer intensification is recorded by just adding 0.5% of CNT. The variation of the injection level (high, medium and low) on the convective transfer is plotted in Figure 11. The transition from a strong injection *C*=10 to a weak injection *C*=1 results in a 19% drop in Nu.

In view of further enhancement on the Nusselt number, it was agreed to adjust the geometrical parameters, in particular the eccentricity (figure 12). Contrary to expectations, the variation of eccentricity does not have a great incidence on the Nusselt number. Moreover, a different behaviour has been detected for positive and negative eccentricity values. Actually, an upward eccentricity variation from 0 to 80% gives rise to a 3% drop in convection transfer, whereas for the same conditions a downward eccentricity ensures a 9% intensification of the heat transfer. In fact, the electrical forces are most intense in the narrow zone of the annulus as the

emitter and collector electrodes approach. Therefore, for an upward eccentricity both electrical and thermal forces act in the somital zone of the annulus generating a low heat exchange zone in the lower half of the inner cylinder. Whereas for downward eccentricity, the electrical forces are stronger in the lower part of the inner cylinder, while the upper part is subject to the action of thermal buoyancy forces, leading to a better heat exchange along the whole inner cylinder.

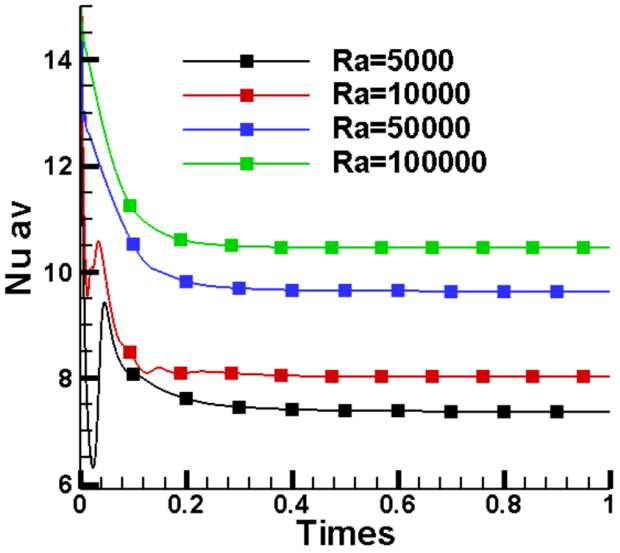

Fig.8. Mean Nusselt number time evolution for Γ=0.2, T=300, C=10, e=0%, ϕ=0.5% and for various Ra values

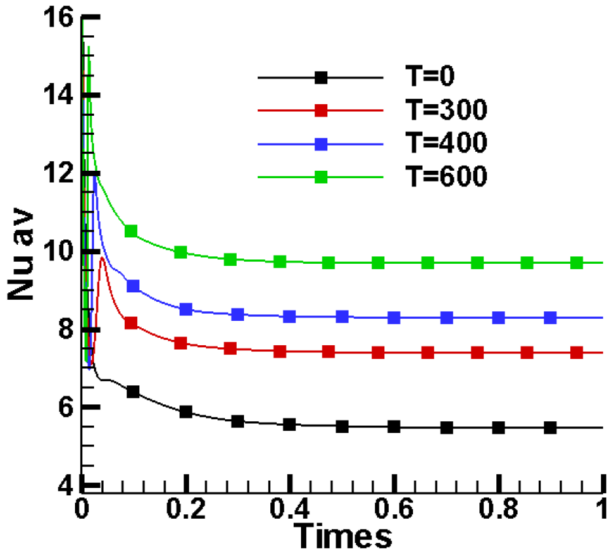

Fig.9. Mean Nusselt number time evolution for Γ=0.2, Ra=5000, C=10, e=0%, ϕ=0.5% and for various T values

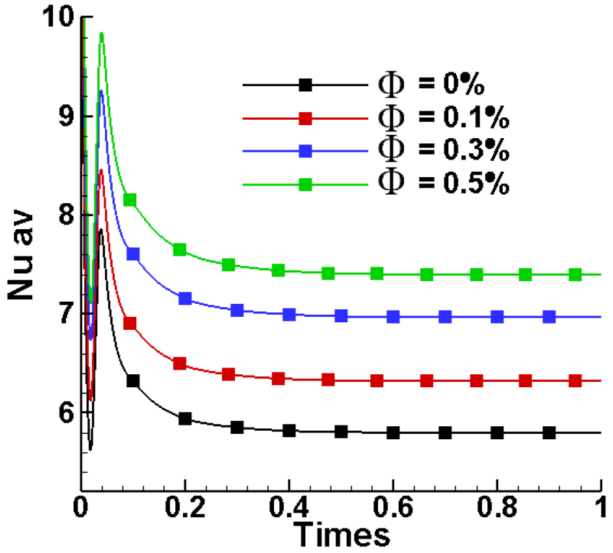

Fig.10. Mean Nusselt number time evolution for Γ=0.2, Ra=5000, T=300, C=10, e=0% and for various Φ values.

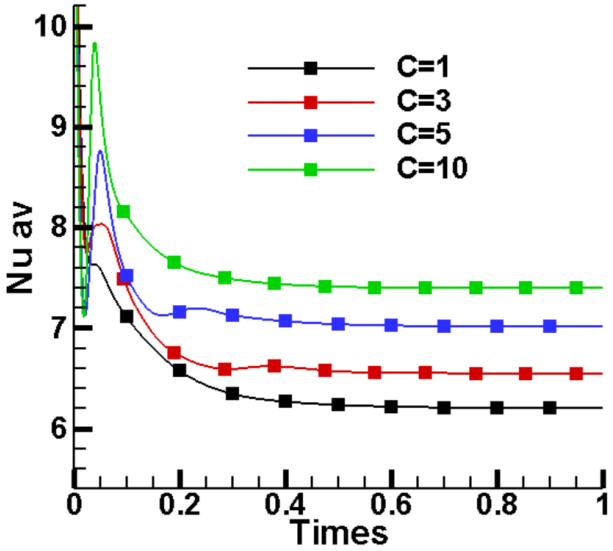

Fig.11. Mean Nusselt number time evolution for Γ=0.2, Ra=5000, T=300, e=0%, ϕ=0.5% and for various C values

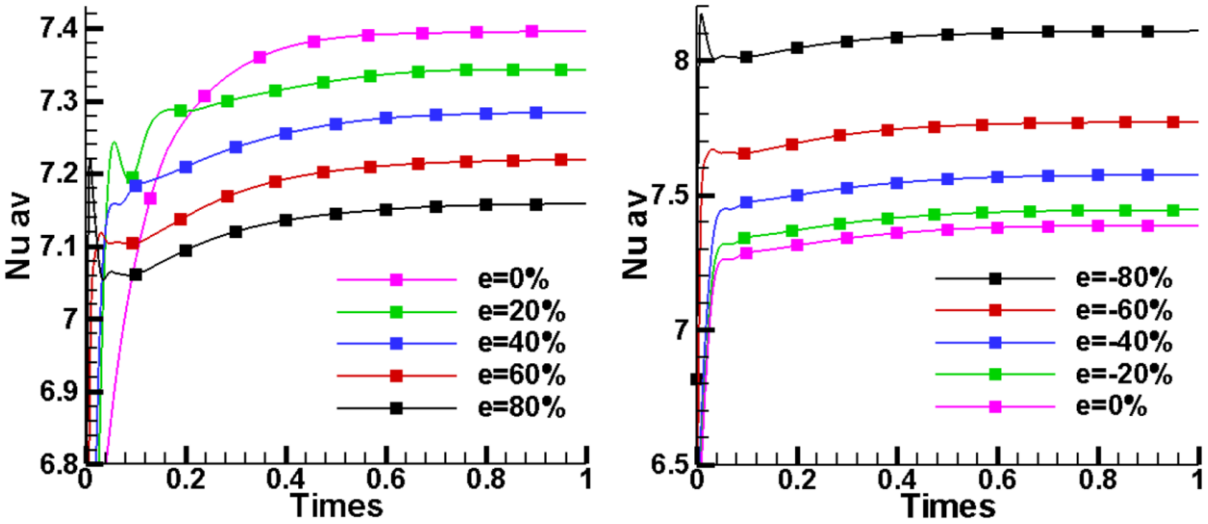

(a) (b)

Fig.12. Mean Nusselt number time evolution for Γ=0.2, Ra=5000, T=300, C=10, ϕ=0.5% and for (a) upwards eccentricity, (b) downwards eccentricity.

The development of mathematical correlations based on statistical approaches is one of the keys to facilitate the resolution of some physical phenomena. These correlations allow the prediction of several parameters giving a huge time saving. In this study, significant dependency relationships have been identified between the average Nusselt number and the simultaneous fluctuations of *Ra*, *T*, *C*, *Γ*, *Φ* and *e*.

After performing several hundred numerical simulations, a multi-parameter empirical correlation was developed based on the regression analysis. Thus, the proposed correlation is valid for thermal Rayleigh number *Ra* between 5,000 and 100,000, thermal Rayleigh *T* between 100 and 600, injection level *C* in the range of 1 to 10, the volume fraction of nanoparticles *Φ* goes from 0.1% to 0.5% and for all eccentricity *e* and radius ratio *Γ* values. Accordingly, the empirical modelled multi-parameter correlation giving the average Nusselt number on the hot inner cylinder can be expressed as follows:

$$Nu_{av} = 0.146\, Ra^{0.116} T^{0.37} C^{0.07} \Gamma^{-0.456} \Phi^{0.11} (e+1)^{-0.052} \quad (27)$$

Comparison tests are required to validate this correlation and to confirm its reliability. In this regard, Figure 13 shows different comparison tests of the average Nusselt number values (Nu_{av}). Several influencing parameters (*Ra*, *T*, *C*, *Γ*, *Φ*, and *e*) were modified to calculate this Nu_{av} either through numerical simulations or through the developed correlation in equation (27). Unless otherwise indicated fig. 13 (a)-(e) are presented for Ra=5000; T=300; C=10; Γ=0.2 and e=0%. Figure 13 demonstrates the excellent agreement between the average Nusselt number calculated numerically and estimated by the correlation, this highlights the strong reliability and accuracy of the developed correlation. Indeed, the maximum error does not exceed 2%, which confirms the reliability and accuracy of the equation (27).

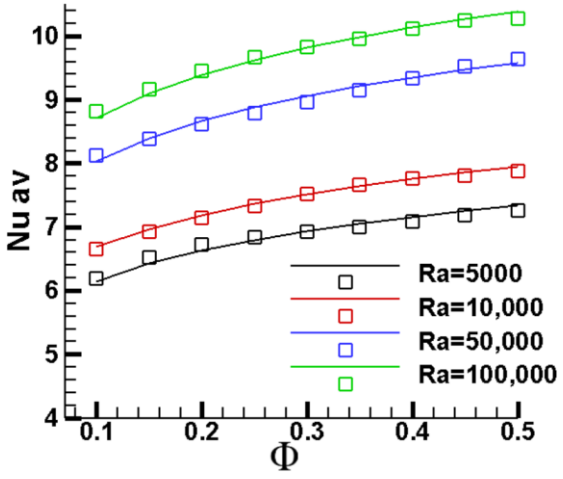

(a)

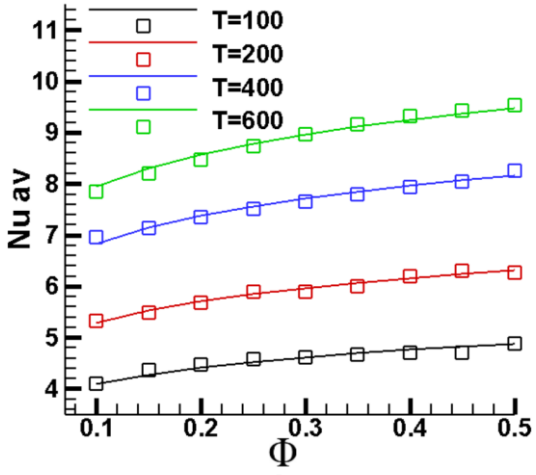

(b)

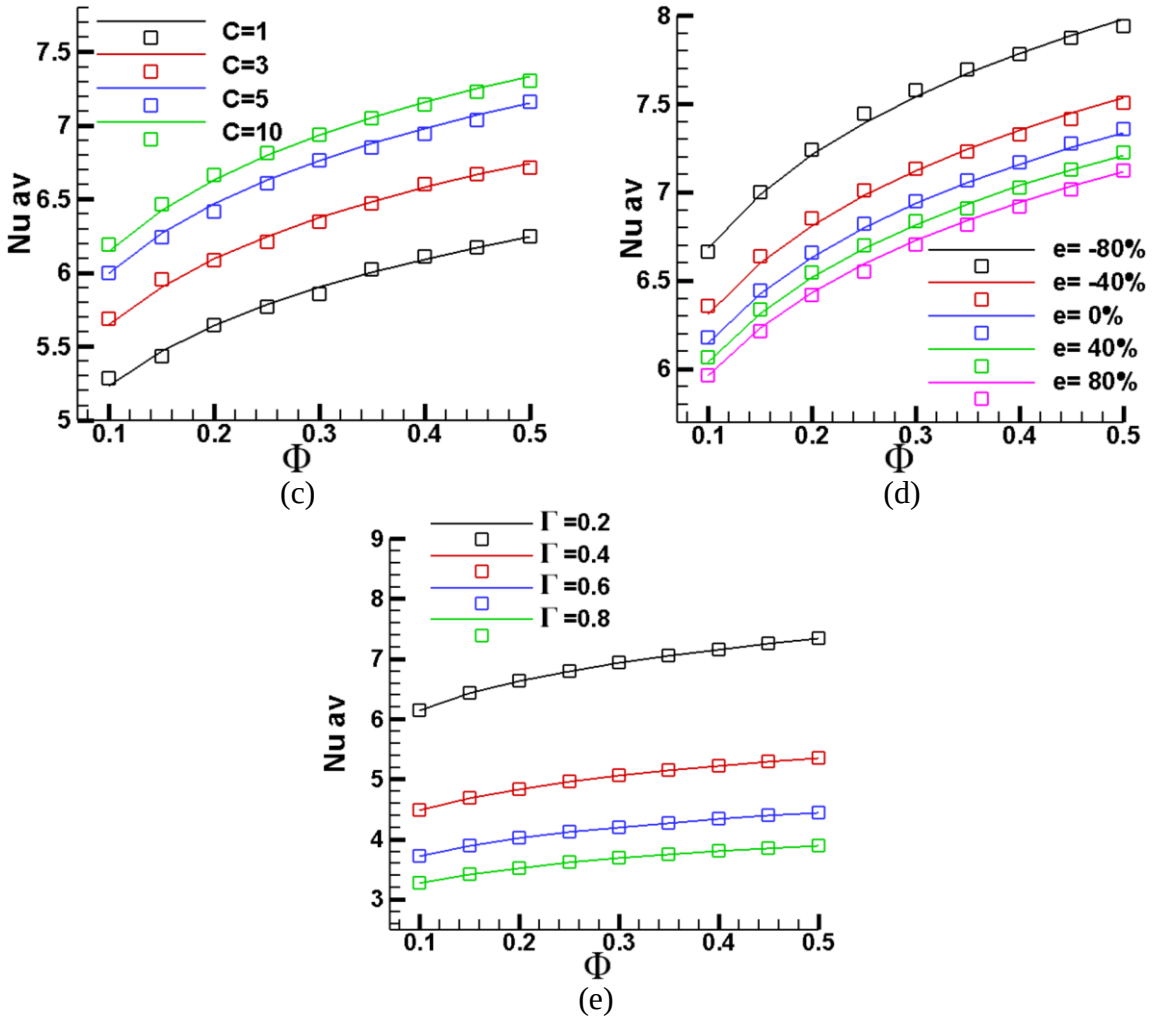

Fig.13. Average Nusselt number Φ for (a) various Ra; (b) various T; (c) various C and (d) various e; (e) various Γ; lines: Correlation values; Symbols: Present numerical results

4. Conclusion

The combined effect of the addition of CNT nanoparticles and the application of an electric field on the improvement of the heat transfer is examined in this work. The geometry considered is an annular layer filled with dielectric oil and bounded by two eccentric or concentric cylinders. The main conclusion that can be drawn is that:

– The flow topography is strongly related to the value of the electrical Rayleigh number. Two different regimes have been detected: a thermal-dominant regime T<300 characterized by two counter-rotating cells with a dead zone of low heat exchange located in the basal zone; and another electrical-dominant regime T>300 characterized

by the development of several counter-rotating cells with a good heat exchange over the whole domain and the disappearance of the dead zone.

- The geometric parameters have a very significant impact on the flow behaviour. Indeed, the cell number and the electric plume number are proportional to the radius ratio "Γ" and inversely proportional to the eccentricity.
- Convective heat transfer can be controlled by thermal and electrical Rayleigh number values. An enhancement of the Nusselt number of 40% and 77% can be achieved by varying Ra from 5000 to 100000 and T from 0 to 600 respectively.
- The addition of 0.5 % in carbon nanotube volume fraction allows the Nusselt number to be enhanced by 27%.
- The eccentricity has also a substantial contribution to the convective transfer. in fact, an upward eccentricity variation from 0 to 80% gives rise to a 3% drop in convection transfer, whereas for the same conditions a downward eccentricity ensures a 9% intensification of the heat transfer

References

[1] Kh. Hosseinzadeh, M. A. Erfani Moghaddam, M. Hatami, D. D. Ganji, et F. Ommi, « Experimental and numerical study for the effect of aqueous solution on heat transfer characteristics of two phase close thermosyphon », *Int. Commun. Heat Mass Transf.*, vol. 135, p. 106129, juin 2022, doi: 10.1016/j.icheatmasstransfer.2022.106129.

[2] M. A. E. Moghaddam, M. R. Hassani Soukht Abandani, Kh. Hosseinzadeh, M. B. Shafii, et D. D. Ganji, « Metal foam and fin implementation into a triple concentric tube heat exchanger over melting evolution », *Theor. Appl. Mech. Lett.*, vol. 12, n^{o} 2, p. 100332, févr. 2022, doi: 10.1016/j.taml.2022.100332.

[3] Kh. Hosseinzadeh, D. D. Ganji, et Fathollah. Ommi, « Effect of SiO2 super-hydrophobic coating and self-rewetting fluid on two phase closed thermosyphon heat transfer

characteristics: An experimental and numerical study », *J. Mol. Liq.*, vol. 315, p. 113748, oct. 2020, doi: 10.1016/j.molliq.2020.113748.
[4] H. Senftleben et W. Braun, « Der Einfluß elektrischer Felder auf den Wärmestrom in Gasen », *Z. Für Phys.*, vol. 102, n° 7, p. 480‑506, juill. 1936, doi: 10.1007/BF01337819.
[5] G. Ahsmann et R. Kronig, « The influence of electric fields on the convective heat transfer in liquids », *Appl. Sci. Res.*, vol. 2, n° 1, p. 235‑244, janv. 1951, doi: 10.1007/BF00411985.
[6] R. Kronig et N. Schwarz, « On the theory of heat transfer from a wire in an electric field », *Flow Turbul. Combust.*, vol. 1, n° 1, p. 35, déc. 1949, doi: 10.1007/BF02120314.
[7] Y. Y. Yan, H. B. Zhang, et J. B. Hull, « Numerical modeling of electrohydrodynamic (ehd) effect on natural convection in an enclosure », *Numer. Heat Transf. Part Appl.*, vol. 46, n° 5, p. 453‑471, sept. 2004, doi: 10.1080/10407780490478461.
[8] Ph. Traoré, A. T. Pérez, D. Koulova, et H. Romat, « Numerical modelling of finite-amplitude electro-thermo-convection in a dielectric liquid layer subjected to both unipolar injection and temperature gradient », *J. Fluid Mech.*, vol. 658, p. 279‑293, sept. 2010, doi: 10.1017/S0022112010001709.
[9] K. Dantchi, T. Philippe, R. Hubert, W. Jian, et L. Christophe, « Numerical simulations of electro-thermo-convection and heat transfer in 2D cavity », *J. Electrost.*, vol. 71, n° 3, p. 341‑344, juin 2013, doi: 10.1016/j.elstat.2012.12.043.
[10] W. Hassen, M. I. Elkhazen, P. Traore, et M. N. Borjini, « Numerical study of the electro–thermo-convection in an annular dielectric layer subjected to a partial unipolar injection », *Int. J. Heat Fluid Flow*, vol. 50, p. 201‑208, déc. 2014, doi: 10.1016/j.ijheatfluidflow.2014.08.003.
[11] W. Hassen, M. N. Borjini, et H. B. Aissia, « Enhanced Heat Transfer by Unipolar Injection of Electric Charges in Differentially Heated Dielectric Liquid Layer », *Fluid Dyn. Mater. Process.*, vol. 8, n° 4, p. 381‑396, 2012, doi: 10.3970/fdmp.2012.008.381.
[12] M. Rezaee, A. A. Taheri, et M. Jafari, « Experimental study of natural heat transfer enhancement in a rectangular finned surface by EHD method », *Int. Commun. Heat Mass Transf.*, vol. 119, p. 104969, déc. 2020, doi: 10.1016/j.icheatmasstransfer.2020.104969.
[13] D. V. Fernandes et Y. K. Suh, « Numerical simulation and design optimization of an electrohydrodynamic pump for dielectric liquids », *Int. J. Heat Fluid Flow*, vol. 57, p. 1‑10, févr. 2016, doi: 10.1016/j.ijheatfluidflow.2015.11.003.
[14] N. Rani et S. K. Tomar, « EHD convection in dielectric micropolar fluid layer », *J. Electrost.*, vol. 78, p. 60‑67, déc. 2015, doi: 10.1016/j.elstat.2015.10.003.
[15] A. Wakif, Z. Boulahia, et R. Sehaqui, « A semi-analytical analysis of electro-thermo-hydrodynamic stability in dielectric nanofluids using Buongiorno's mathematical model together with more realistic boundary conditions », *Results Phys.*, vol. 9, p. 1438‑1454, juin 2018, doi: 10.1016/j.rinp.2018.01.066.
[16] H. M. Maghrabie *et al.*, « Intensification of heat exchanger performance utilizing nanofluids », *Int. J. Thermofluids*, vol. 10, p. 100071, mai 2021, doi: 10.1016/j.ijft.2021.100071.
[17] R. Mohammad et R. Kandasamy, « Nanoparticle shapes on electric and magnetic force in water, ethylene glycol and engine oil based Cu, Al 2 O 3 and SWCNTs », *J. Mol. Liq.*, vol. 237, p. 54‑64, juill. 2017, doi: 10.1016/j.molliq.2017.04.045.
[18] B. Mallick et J. C. Misra, « Peristaltic flow of Eyring-Powell nanofluid under the action of an electromagnetic field », *Eng. Sci. Technol. Int. J.*, vol. 22, n° 1, p. 266‑281, févr. 2019, doi: 10.1016/j.jestch.2018.12.001.

[19] L. Kolsi, A. A. A. A. Alrashed, K. Al-Salem, H. F. Oztop, et M. N. Borjini, « Control of natural convection via inclined plate of CNT-water nanofluid in an open sided cubical enclosure under magnetic field », *Int. J. Heat Mass Transf.*, vol. 111, p. 1007‑1018, août 2017, doi: 10.1016/j.ijheatmasstransfer.2017.04.069.
[20] R. Chand, « Electro-thermal convection in a Brinkman porous medium saturated by nanofluid », *Ain Shams Eng. J.*, vol. 8, n° 4, p. 633‑641, déc. 2017, doi: 10.1016/j.asej.2015.10.008.
[21] Kh. Hosseinzadeh, So. Roghani, A. R. Mogharrebi, A. Asadi, et D. D. Ganji, « Optimization of hybrid nanoparticles with mixture fluid flow in an octagonal porous medium by effect of radiation and magnetic field », *J. Therm. Anal. Calorim.*, vol. 143, n° 2, p. 1413‑1424, janv. 2021, doi: 10.1007/s10973-020-10376-9.
[22] Kh. Hosseinzadeh, E. Montazer, M. B. Shafii, et D. D. Ganji, « Heat transfer hybrid nanofluid (1-Butanol/MoS_2–Fe_3O_4) through a wavy porous cavity and its optimization », *Int. J. Numer. Methods Heat Fluid Flow*, vol. 31, n° 5, p. 1547‑1567, mai 2021, doi: 10.1108/HFF-07-2020-0442.
[23] A. Kasaeipoor, E. H. Malekshah, et L. Kolsi, « Free convection heat transfer and entropy generation analysis of MWCNT-MgO (15% − 85%)/Water nanofluid using Lattice Boltzmann method in cavity with refrigerant solid body-Experimental thermo-physical properties », *Powder Technol.*, vol. 322, p. 9‑23, déc. 2017, doi: 10.1016/j.powtec.2017.08.061.
[24] F. Asadzadeh, M. Nasr Esfahany, et N. Etesami, « Natural convective heat transfer of Fe3O4/ethylene glycol nanofluid in electric field », *Int. J. Therm. Sci.*, vol. 62, p. 114‑119, déc. 2012, doi: 10.1016/j.ijthermalsci.2011.11.010.
[25] M. Sheikholeslami, T. Hayat, A. Alsaedi, et S. Abelman, « Numerical analysis of EHD nanofluid force convective heat transfer considering electric field dependent viscosity », *Int. J. Heat Mass Transf.*, vol. 108, p. 2558‑2565, mai 2017, doi: 10.1016/j.ijheatmasstransfer.2016.10.099.
[26] M. Sheikholeslami et M. M. Bhatti, « Active method for nanofluid heat transfer enhancement by means of EHD », *Int. J. Heat Mass Transf.*, vol. 109, p. 115‑122, juin 2017, doi: 10.1016/j.ijheatmasstransfer.2017.01.115.
[27] W. Hassen, L. Kolsi, H. A. Mohammed, K. Ghachem, M. Sheikholeslami, et M. A. Almeshaal, « Transient electrohydrodynamic convective flow and heat transfer of MWCNT - Dielectric nanofluid in a heated enclosure », *Phys. Lett. A*, vol. 384, n° 28, p. 126736, oct. 2020, doi: 10.1016/j.physleta.2020.126736.
[28] W. Hassen, M. I. Elkhazen, P. Traore, et M. N. Borjini, « Charge injection in horizontal eccentric annuli filled with a dielectric liquid », *Eur. J. Mech. - BFluids*, vol. 72, p. 691‑700, nov. 2018, doi: 10.1016/j.euromechflu.2018.08.009.
[29] W. Hassen, H. F. Oztop, L. Kolsi, M. N. Borjini, et N. Abu-Hamdeh, « Analysis of the electro-thermo-convection induced by a strong unipolar injection between two concentric or eccentric cylinders », *Numer. Heat Transf. Part Appl.*, vol. 71, n° 7, p. 789‑804, avr. 2017, doi: 10.1080/10407782.2017.1308725.
[30] J. L. Lara, F. Pontiga, et A. Castellanos, « Stability analysis of a Taylor–Couette flow of insulating fluid subjected to radial unipolar injection of charge », *Phys. Fluids*, vol. 10, n° 12, p. 3088‑3098, déc. 1998, doi: 10.1063/1.869837.
[31] S. U. Ilyas, R. Pendyala, et M. Narahari, « Stability and thermal analysis of MWCNT-thermal oil-based nanofluids », *Colloids Surf. Physicochem. Eng. Asp.*, vol. 527, p. 11‑22, août 2017, doi: 10.1016/j.colsurfa.2017.05.004.
[32] K. Luo, J. Wu, H.-L. Yi, et H.-P. Tan, « Numerical investigation of heat transfer enhancement in electro-thermo-convection in a square enclosure with an inner circular

cylinder », *Int. J. Heat Mass Transf.*, vol. 113, p. 1070‑1085, oct. 2017, doi: 10.1016/j.ijheatmasstransfer.2017.06.003.
[33] K. Kahveci, « Buoyancy Driven Heat Transfer of Nanofluids in a Tilted Enclosure », *J. Heat Transf.*, vol. 132, n° 6, p. 062501, juin 2010, doi: 10.1115/1.4000744.
[34] M. N. Borjini, A. Abidi, et H. B. Aissia, « Prediction of Unsteady Natural Convection within a Horizontal Narrow Annular Space Using the Control-Volume Method », *Numer. Heat Transf. Part Appl.*, vol. 48, n° 8, p. 811‑829, nov. 2005, doi: 10.1080/10407780500196576.
[35] A. Bejan, *Convection heat transfer*. John Wiley & Sons, Inc., 2013.
[36] P. A. Vázquez, G. E. Georghiou, et A. Castellanos, « Numerical analysis of the stability of the electrohydrodynamic (EHD) electroconvection between two plates », *J. Phys. Appl. Phys.*, vol. 41, n° 17, p. 175303, août 2008, doi: 10.1088/0022-3727/41/17/175303.
[37] W. Hassen, M. N. Borjini, P. Traore, et H. Ben Aissia, « Electroconvection between coaxial cylinders of arbitrary ratio subjected to strong unipolar injection », *J. Electrost.*, vol. 71, n° 5, p. 882‑891, oct. 2013, doi: 10.1016/j.elstat.2013.07.002.
[38] T. H. Kuehn et R. J. Goldstein, « An experimental and theoretical study of natural convection in the annulus between horizontal concentric cylinders », *J. Fluid Mech.*, vol. 74, n° 4, p. 695‑719, avr. 1976, doi: 10.1017/S0022112076002012.
[39] J. Wu, P. A. Vázquez, P. Traoré, et A. T. Pérez, « Finite amplitude electroconvection induced by strong unipolar injection between two coaxial cylinders », *Phys. Fluids*, vol. 26, n° 12, p. 124105, déc. 2014, doi: 10.1063/1.4903284.